

errors. Uncertainties in the argon abundance and the cold-trapping constraint applied in the tropopause region also contributed to the errors in the estimated CH_4 mole fraction. The use of the pure rotational lines of CH_4 in the far-infrared (fig. S2B) eliminates many of these ambiguities. The line-formation region is in the stratosphere between 3 and 20 mbar (140 to 80 km altitude), which mostly lies between the two regions accessible to direct-temperature sounding, the upper troposphere and tropopause region between 500 and 50 mbar (20 to 60 km), and the upper stratosphere between 5 and 0.5 mbar (130 to 230 km). Nevertheless, interpolation between the two altitude ranges constrains the temperatures sufficiently to make an improved determination of the stratospheric CH_4 abundance. The optically thick ν_4 band is not too sensitive to the CH_4 abundance, but is more sensitive to the stratospheric temperatures, because it is on the Wien tail of the Planck function. The rotational lines are almost optically thin, and therefore they are more sensitive to the stratospheric CH_4 abundance but less sensitive to temperature, because they lie at wave numbers below those at the peak emission (fig. S1) (30). Figure S4 illustrates fits for synthetic spectra with different CH_4 mole fractions. The best fit in a least-squares sense to all the rotational lines corresponds to a mole fraction of $(1.6 \pm 0.5) \times 10^{-2}$. This is comparable to the mole fraction determined at 1000- to 1200-km altitude from remote-sensing and in situ measurements (table S1), indicating that CH_4 is fairly well mixed up to these altitudes.

In addition to containing CH_4 , the far-infrared contains rotational lines of stratospheric emission from CO and HCN (fig. S2A). The rotational line-formation region of CO is similar to that of CH_4 . We find from a least-

squares fit of all the lines observed in independent selections of spectra from the T0 and TB flybys that the CO mole fraction is $(4.5 \pm 1.5) \times 10^{-5}$, assuming that it is uniform with altitude (31). This is consistent with the determination $[(5.0 \pm 1.0) \times 10^{-5}]$ by Gurwell and Muhleman (32), and marginally consistent with what Hidayat *et al.* (33) inferred below the 1-mbar level from disk-averaged heterodyne millimeter observations $[(2.5 \pm 0.5) \times 10^{-5}]$. Within the errors, it is also consistent with the tropospheric value $[(3.2 \pm 1.0) \times 10^{-5}]$ derived from 5- μm spectra (34), although one cannot rule out that the stratosphere has a higher concentration. One might expect the mole fractions of CO in the stratosphere and troposphere to be more or less equal, because CO does not condense at the temperatures and abundances observed, and the time constant for photochemical adjustment under current conditions is $\sim 10^9$ years (4).

References and Notes

- G. F. Lindal *et al.*, *Icarus* **53**, 348 (1983).
- D. M. Hunten *et al.*, in *Saturn*, T. Gehrels, M. S. Matthews, Eds. (Univ. of Arizona Press, Tucson, AZ, 1984), pp. 671-759.
- R. E. Samuelson, N. R. Nath, A. Borysow, *Planet. Space Sci.* **45**, 959 (1997).
- Y. L. Yung, M. Allen, J. P. Pinto, *Astrophys. J. (Suppl.)* **55**, 465 (1984).
- D. Toubanc *et al.*, *Icarus* **113**, 2 (1995).
- E. H. Wilson, S. K. Atreya, *J. Geophys. Res.* **109**, E06002, 10.1029/2003JE002181 (2004).
- F. M. Flasar, R. E. Samuelson, B. J. Conrath, *Nature* **292**, 693 (1981).
- F. M. Flasar, B. J. Conrath, *Icarus* **85**, 346 (1990).
- A. Coustenis, B. Bézard, *Icarus* **115**, 126 (1995).
- V. Kunde *et al.*, in *Cassini/Huygens: A Mission to the Saturnian Systems*, L. Horn, Ed. (SPIE Proceedings, The International Society for Optical Engineering, Bellingham, WA, 1996), pp. 162-177.
- F. M. Flasar *et al.*, *Space Sci. Rev.* **115**, 169 (2004).
- A. Coustenis *et al.*, *Icarus* **161**, 383 (2003).
- W. B. Hubbard *et al.*, *Astron. Astrophys.* **269**, 541 (1993).
- B. Sicardy *et al.*, *Icarus* **142**, 357 (1999).
- R. V. Yelle, *Astrophys. J.* **383**, 380 (1991).

- Materials and methods are available as supporting material on Science Online.
- F. M. Flasar, *Planet. Space Sci.* **46**, 1125 (1998).
- A. Bouchez, thesis, California Institute of Technology (2004); available at www.gps.caltech.edu/~antonin/thesis/.
- F. M. Flasar *et al.*, *Science* **307**, 1247 (2005).
- F. Hourdin *et al.*, *Icarus* **117**, 358 (1995).
- B. Bézard, A. Coustenis, C. P. McKay, *Icarus* **113**, 267 (1995).
- F. Hourdin, S. Lebonnois, D. Luz, P. Rannou, *J. Geophys. Res.* **109**, E12005, 10.1029/2004JE002282 (2004).
- S. Lebonnois, D. Toubanc, F. Hourdin, P. Rannou, *Icarus* **152**, 384 (2001).
- Y. L. Yung, *Icarus* **72**, 468 (1987).
- M. R. Schoeberl, M. R. Hartman, *Science* **251**, 46 (1991).
- J. T. Bacmeister, M. R. Schoeberl, M. E. Summers, J. R. Rosenfeld, X. Zhu, *J. Geophys. Res.* **100**, 11669 (1995).
- H. G. Roe, I. de Pater, C. P. McKay, *Icarus* **169**, 440 (2004).
- J. I. Moses *et al.*, *Icarus* **143**, 244 (2000).
- D. Strobel, *Planet. Space Sci.* **30**, 839 (1982).
- A. Coustenis *et al.*, *Icarus* **102**, 240 (1993).
- To fit the CO rotational lines, we also had to fit the HCN lines. To do so, we used the vertical profile derived by Marten *et al.* (35) from disk-averaged millimeter observations, but scaled by a constant factor, $2.5^{+1.5}_{-1.1}$ (where $+1.5$ and -1.1 are the error values) for a selection of T0 spectra centered at 7°S and 2.8 ± 1 for a selection of TB spectra centered at 17°N .
- M. A. Gunwell, D. O. Muhleman, *Icarus* **117**, 375 (1995).
- T. Hidayat, A. Marten, B. Bézard, D. Gautier, *Icarus* **133**, 109 (1998).
- E. Lellouch *et al.*, *Icarus* **162**, 125 (2003).
- A. Marten, T. Hidayat, Y. Biraud, R. Moreno, *Icarus* **158**, 532 (2002).
- S. Albricht, M. H. Elliott, and J. S. Tingley assisted with instrument commanding and data processing; D. Crick, M. de Cates, and S. Brooks assisted with observation designs; and N. Stone helped with data analysis. We acknowledge support from the NASA Cassini Project, the British Particle Physics and Astronomy Research Council, the Centre National d'Études Spatiales (CNES), and the Institut National des Sciences de l'Univers (CNRS/INSU).

Supporting Online Material

www.sciencemag.org/cgi/content/full/308/5724/975/DC1

Materials and Methods

Figs. S1 to S4

Table S1

References

16 February 2005; accepted 14 April 2005
10.1126/science.1111150

REPORT

The Cassini UVIS Stellar Probe of the Titan Atmosphere

Donald E. Shemansky,^{1*} A. Ian F. Stewart,² Robert A. West,³ Larry W. Esposito,² Janet T. Hallett,¹ Xianming Liu¹

The Cassini Ultraviolet Imaging Spectrometer (UVIS) observed the extinction of photons from two stars by the atmosphere of Titan during the Titan flyby. Six species were identified and measured: methane, acetylene, ethylene, ethane, diacetylene, and hydrogen cyanide. The observations cover altitudes from 450 to 1600 kilometers above the surface. A mesopause is inferred from extraction of the temperature structure of methane, located at 615 km with a temperature minimum of 114 kelvin. The asymptotic kinetic temperature at the top of the atmosphere determined from this experiment is 151 kelvin. The higher order hydrocarbons and hydrogen cyanide peak sharply in abundance and are undetectable below altitudes ranging from 750 to 600 km, leaving methane as the only identifiable carbonaceous molecule in this experiment below 600 km.

On 13 December 2004, the Cassini UVIS observed the occultation of two stars, Shaula (λ Sco) and Spica (α Vir) near the end of the

second Titan flyby (labeled T_B). Both measurements of atmospheric transmission were obtained in egress: Spica was in the northern

hemisphere over a range of latitudes and Shaula at a southern latitude, -36° (fig. S1). Observations were made with the extreme ultraviolet (EUV) and the far ultraviolet (FUV) UVIS channels (1). Data from Spica were compromised by spacecraft pointing drift but provide useful comparative atmospheric structural information at lower altitudes (2). The spectral range of the FUV observations (110 nm to 190 nm) is effective for the identification and determination of the hydrocarbon species abundances. These complement and extend solar occultation results from Voyager 1 and 2 in 1980 to 1981 (3, 4) into the range 900 to 1200 km for CH_4 . Our data

cover altitudes of 450 to 1600 km, showing the presence of a mesopause at 615 km. The distribution of higher order hydrocarbons and HCN in the results reported here shows a distinct divergence from inferences in the recent reanalysis (4) of the Voyager data.

We begin the description of the properties of the photon transmission at low altitudes, where the stellar photons are first detected in egress. Although the Spica results were affected by pointing drift at high altitude, a useful comparison can be made with Shaula at low altitudes (2), where transmission properties of species, other than the N_2 , hydrocarbons, and HCN identified here, determine the observed photon flux. In the spectral region 180 to 190 nm defined as c (2), extinction by the carbonaceous species (and N_2) considered here is negligible. The Spica occultation occurred in the northern hemisphere over a latitude range of 70° to -30° , whereas Shaula occurred at a nearly constant -36° latitude (fig. S1). Measurable signal begins (first light) in c at 293 km in Shaula data and 279 km in Spica (fig. S2). The extinction of radiation in region c below 300 km and extending to below 200 km is attributed to species other than those identified in the UVIS spectra. The altitude difference (14 km) in first light between Shaula and Spica is attributed to global nonuniformity in atmospheric structure, because the asymptotic scale heights in the two data sets differ by 50% (11.1 and 7.5 km), with extinction a factor of 4 to 5 deeper for Shaula compared with Spica at 360 km (fig. S2), whereas the transmission curves match almost exactly above 500 km. The species in this region of the atmosphere do not have an identified spectral signature but are important components affecting the thermal and dynamic structure (5, 6) that constitutes a major target of the Cassini Program. Aerosols are probably responsible for the extinction in this region. The narrow feature at 510 km in the Shaula profile may be the scattering haze seen in reflected sunlight in the Cassini Imaging Science Subsystem (ISS) (7). The data analyzed here are composed of sets of five contiguous exposure records that contain the spectral signals integrated over intervals of approximately 20 km of vertical atmospheric structure. The effective impact parameter altitude for analysis of each group of five measurements is determined by weighting against the estimated atmospheric scale height. The minimum scale height in the CH_4 data is ~ 40 km.

The reduction process to obtain species line-of-sight (LOS) abundances, by necessity,

was carried out by simulation of the instrument response to modeled spectra, because of substantial internal scattering effects in the combined optical and detector system. The absorption structures of the six species recognized in the data have distinctive spectral shapes, but they are heavily overlapped. The data-reduction process was therefore carried out by iterative fitting of each of the observed absorption spectra by forward synthesis (2). Figure 1 shows the derived altitude distribution of abundance (molecules cm^{-2}). Uncertainties in the derived values, including a large component attributed to problems with the experimental cross sections of the higher hydrocarbons and HCN discussed in the supplementary online materials (2), are shown in Fig. 1. The photoabsorption cross sections (8–20) used here are the most recently available. The absorption spectra allow measurement of six species in the Titan upper atmosphere: CH_4 , C_2H_2 , C_2H_4 , C_2H_6 , HCN, and C_4H_2 (methane, acetylene, ethylene, ethane, hydrogen cyanide, and diacetylene) (Fig. 1).

The most important properties of the derived abundances from the present experiment plotted in Fig. 1 are the presence of a distinct change in slope in all of the species near 800 km altitude and the sudden leveling off of the LOS abundances of the higher hydrocarbons and HCN below 750 and 600 km. Model calculations fitting the CH_4 abundance data are shown plotted over the data in Fig. 1. The model fit to the data provides an extraction of the density, fundamental scale height, and temperature profiles of this species. This detailed model calculation, described below, was limited to CH_4 in the present work. The leveling off in the abundances of the higher order hydrocarbons and HCN below 750 and 600 km is an indicator that these species are not measurably present below these altitudes. The latter result is strongly divergent from the recent reanalysis of the Voyager solar occultation (4). The observed changes in the profiles

of the higher order hydrocarbon and HCN distribution indicate that these species are subject to strong photochemical source-and-sink processes. Figure 1 includes abundance values for CH_4 from the Voyager experiment (4) and calculated LOS values from the Cassini Ion Neutral Mass Spectrometer (INMS) experiment inbound density measurements from the first Titan flyby (labeled T_A) provided by Yelle (21).

We obtain values of species number densities from the abundances shown in Fig. 1 by assuming that the atmosphere is hemispherically uniform, because the observations are intrinsically an integration along the LOS through the extent of the atmosphere. The derivation of the density, scale height, and temperature distribution of CH_4 is obtained assuming a hydrostatic atmosphere. The transmission of the stellar flux through the atmosphere is developed through the relations

$$\ln\left(\frac{I_v}{I_v^0}\right) = -2 \int_0^\ell k_v d\ell \quad (1)$$

$$k_v = \sigma_v n(\ell) \quad (2)$$

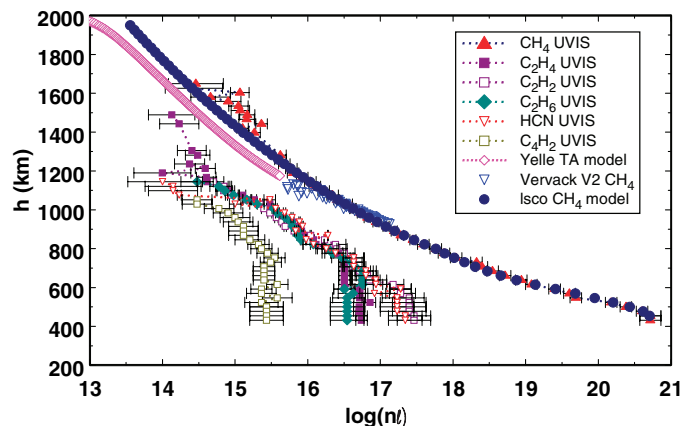
$$\tau_v = k_v \bar{\ell} \quad (3)$$

$$\eta = \bar{n}(\ell) \bar{\ell} \quad (4)$$

where ℓ (cm) is location along the path of the flux through the atmosphere, k_v is the absorption coefficient (cm^{-1}), τ_v is optical depth, $n(\ell)$ (cm^{-3}) is gas number density, σ_v (cm^2) is the scattering or absorption cross section, I_v^0 is the incident differential stellar flux, and I_v is the emergent differential flux observed by the spectrograph. The quantity $\eta_i(h)$ (cm^{-2}) is the abundance for species i , and the bar quantities are effective values.

We based our analysis on the quantity I_v/I_v^0 so that no absolute values of stellar flux are required. An example of a $\ln(I_v/I_v^0)$ spectrum containing observed data compared with the model simulation used to extract absorber

Fig. 1. Derived abundances of hydrocarbon species and HCN identified in the UVIS occultation of Shaula at Titan flyby T_B . The data are plotted in base 10 logarithm of abundance (cm^{-2}) against line-of-sight impact parameter h . A model fit to the CH_4 data is shown superimposed, which has allowed derivation of temperature, scale height distribution, and number density as functions of altitude. The calculated abundance of CH_4 derived from the INMS data (21) from flyby T_A (fig. S1) is also included. The Vervack *et al.* (4) derivation of CH_4 abundance from the Voyager encounter is also plotted, indicating close conformance with the INMS-derived values (21).



¹Department of Aerospace Engineering, University of Southern California, University Park, Los Angeles, CA 90089, USA. ²University of Colorado, Laboratory for Atmospheric and Space Physics, Boulder, CO 80303, USA. ³Jet Propulsion Laboratory, Pasadena, CA 91109, USA.

*To whom correspondence should be addressed. E-mail: dons@hippolyta.usc.edu

abundances, $\eta_i(h)$, is shown in Fig. 2. Reducing the values of $\eta_i(h)$ to atmospheric vertical density distribution requires, effectively, differentiation of $\eta_i(h)$ as a function of LOS impact parameter, h , the minimum vertical altitude in the atmosphere. Direct differentiation of $\eta_i(h)$ is not practical, and in practice the density must be derived through an iterative forward-modeling process. The fundamental equation connecting pressure P and mass density $\rho_i(h)$ at altitude h is

$$dP = -g\rho dh \quad (5)$$

$$\frac{dP}{P} = -\frac{1}{H(h)} dh \quad (6)$$

$$H(h) = \frac{kT(h)}{\bar{m}(h)g(h)} \quad (7)$$

$$\rho_i(h) = n_i(h)m_i(h) \quad (8)$$

where H is scale height, and $g(h)$, $m(h)$, and $T(h)$ (gravitational acceleration, effective mass, and temperature, respectively) are altitude-dependent quantities, as indicated. The number density $n_i(h)$ is obtained from

$$\rho_i(h) = \frac{\rho_i(h_0)T(h_0)}{T(h)} \exp \left[\int_{h_0}^h -\frac{\bar{m}(h)}{k} \frac{g(h)dh}{T(h)} \right] \quad (9)$$

$n_i(h)$ must then be derived from $\eta_i(h)$ through the relation

$$\eta_i(h) = 2 \cdot \int_0^\ell n(\ell, h) d\ell \quad (10)$$

These equations relate to a hydrostatic atmosphere and for this reason are limited in applicability to the globally nonuniform Titan atmosphere. If the atmosphere is not simple, as is the case for Titan, Eq. 10 must be solved iteratively on the distribution of $\eta_i(h)$ to extract $n_i(h)$, $m(h)$, $T(h)$, and ultimately $H(h)$ [$g(h)$ is, of course, a known quantity]. The quantity $m(h)$ has a complex dependence on atmospheric dynamics in this case (22), but there are constraints that limit behavior. Low in the atmosphere, it is safe to assume a fully mixed structure, so $m(h \ll \cdot)$ is fixed to the value 28 atomic mass units (amu), determined by the dominant N_2 component. It is this factor that constrains $T(h)$ for CH_4 in our analysis at altitudes up to 700 km. The derived temperature and scale height distribution for CH_4 is given in Fig. 3. Solutions to higher altitude then involve a collision frequency and bulk motion (diffusion) dependent transition to the asymptotic diffusive-separation value of $m(h) = 16$ amu for CH_4 . The departure from a mixed to diffusively separated atmosphere is indicated in Fig. 3 in the plot of the inferred N_2 scale height profile, shown as open triangles above 800 km, to be compared to the closed

triangles. This result does not coincide with the analysis of the Cassini INMS experiment (23) but does agree approximately with recent model calculations (24–26).

The atmospheric kinetic temperature extracted from the derived CH_4 abundance declines rapidly with increasing altitude from 173 K at 450 km to 114 K at 615 km and rises at higher altitudes to 151 K at the top of the atmosphere. The location of the minimum temperature coincides approximately with the location of maximum abundance of HCN and the higher order hydrocarbons and marks the location of maximum infrared radiative cooling to space (Fig. 1). The kinetic temperature at the top of the atmosphere is, within 5%, in agreement with the results of the in situ Cassini INMS (23) (149 K) at the first Cassini encounter (T_A). Above 1200 km, the scale height depends on altitude according to the variation in $g(h)$, with constant $m(h \gg \cdot) = 16$ amu and kinetic temperature rising from 148 K to a terminal 151 K. The modeled values of

CH_4 abundance shown in Fig. 1 are based on the iteratively determined CH_4 scale heights and temperatures given in Fig. 3. The sharp decline in temperature from an altitude of 450 km to 615 km required to fit the Shaula CH_4 abundance distribution has a temperature lapse rate of -1 K/km at 450 km and a mean of -0.37 K/km to the mesopause (for Earth, -6 K/km between stratopause and mesopause), compared with a predicted adiabatic lapse of -0.94 K/km. Figure 3 includes a plot of the Voyager results from the radio occultation (27) measurements showing the derived lower atmosphere temperature structure from ground level to 200 km, leaving a gap between 200 km and 450 km with the present results. The Yelle *et al.* (28) recommended and minimum engineering models of vertical temperature distribution are also shown in Fig. 3.

The solution of Eq. 10, confined by the abundance values derived from the observations, to obtain the temperature and scale height profiles proceeds through the integra-

Fig. 2. Example of observed Shaula transmission spectrum from the Cassini UVIS FUV spectrograph, compared with a model synthesis of the absorbers CH_4 , C_2H_2 , C_2H_4 , C_2H_6 , HCN, and C_4H_2 at weighted mean impact parameter $h = 868.4$ km. Abundance values of the absorbers (cm^{-2}) are given. A distinct deficiency in the fit to the observed transmission spectrum appears at 144.5 nm and 164.5 nm, identified as Rydberg resonances in C_4H_2 . The experimental data for C_4H_2 are saturated in these features and cannot reproduce the observed spectrum at these locations. At deeper locations in the atmosphere, modeled C_2H_2 resonances that are satisfactory in the spectrum shown here are no longer adequate because of temperature dependence in the absorption properties. Structure near the H Ly α line in the stellar spectra is caused by the dominance of internal instrumental scattering where the stellar flux is negligible.

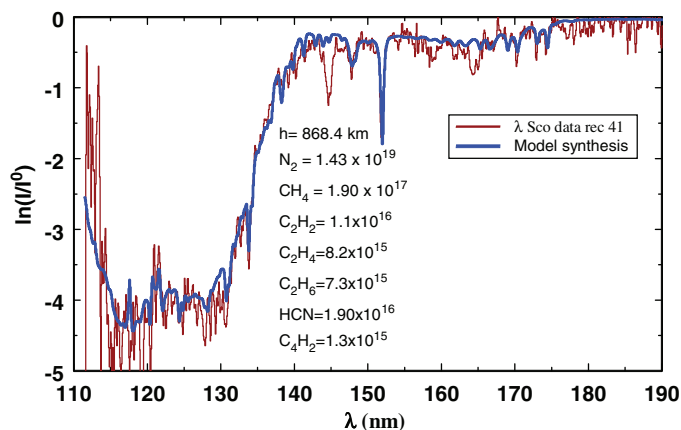
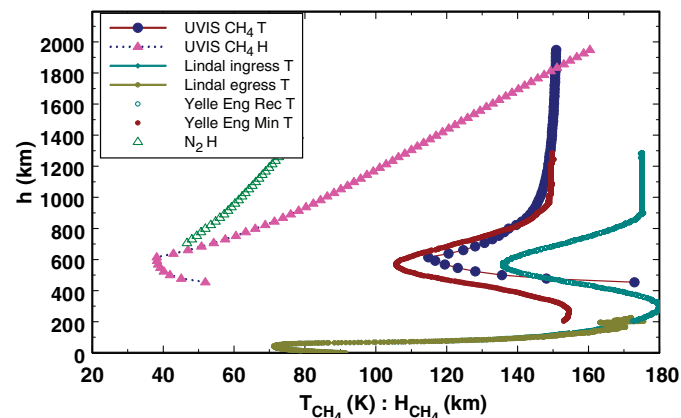


Fig. 3. Scale height (H) and temperature (T) derived for CH_4 from a model fit to the UVIS FUV abundance data shown in Fig. 1. The inferred scale height for N_2 is shown, indicating the location of departure from a mixed atmosphere in this analysis. The Voyager radio occultation results (27), giving temperature distribution from 0 to 200 km, are included for comparison, along with the Yelle *et al.* (28) recommended and minimum engineering models. The recommended model (28) is based on the original analysis of the Voyager Titan occultation, which reported a top-of-atmosphere temperature of 178 K.



tion of Eq. 9, directly provides an extraction of the species density distribution. The densities for CH₄ obtained in this way are shown in Fig. 4. The densities of the remaining species are estimated by rough approximation to the modeling process described here for CH₄. The densities at selected altitudes for the measured species, compared with recent model calculations (24), are shown in Table 1. The analysis from the Vervack *et al.* (4, 29) work on the Voyager encounter data is included in Fig. 4. A model fit to the INMS (23) data, beginning at 1174 km, is also shown in Fig. 4, extended through the post-T_A model calculations by Yelle (21). The INMS (23) densities fall below the present values by a factor of 2 at 1200 km. Important aspects of the comparison of these results are that the INMS-Yelle CH₄ densities parallel the present values

above 1200 km (which indicates both to be diffusively separated distributions at essentially the same temperature) and that below 1200 km, the Vervack *et al.* and INMS-Yelle results show smaller CH₄ scale heights than the present work (Fig. 4). This trend is consistent with the high-altitude transition to a mixed atmosphere in the former inferred isothermal structure, compared with the downwardly decreasing temperature in the present results with a significantly lower homopause. It is plausible that these differences are driven by atmospheric dynamics (30, 31), because the Voyager and INMS observations were obtained across the terminator and the UVIS LOS was primarily in the dark southern hemisphere atmosphere (fig. S1). We regard this difference as probably driven by global nonuniformity in atmospheric structure rather than reflecting actual dif-

ferences in data extraction in the two experiments, but there is certainly room for error on either side of this issue. The Voyager ingress and egress results straddle Shaula at 900 km (Fig. 4). Model (24) calculations agree within uncertainty with our determination of CH₄ density at the lower altitudes, but the model shows a trend (Fig. 4 and Table 1) from low to high altitude consistent with differences in applied temperature structure. In contrast, our data show greater densities than the model (24) for the higher hydrocarbons and HCN by factors of at least 2 (Table 1). The consistently larger derived densities for all of these species suggest that the differences are physically real. The Cassini UVIS data also imply that the lower atmosphere is layered (Fig. 1) in the higher order hydrocarbons and HCN. Below 600 km, the density of these species drops precipitously to undetectable levels, to mixing ratios four to six orders of magnitude below that of CH₄. This result is in strong disagreement with inferred measured densities of higher order hydrocarbons and HCN from the Voyager experiment (4) below 600 km. The implied lack of efficient radiators below 600 km provides a primary reason for the rise in the derived kinetic temperature below 615 km shown in Fig. 1.

This structure is different from that implied in photochemical models of the Titan atmosphere, in large part because atmospheric hazes are the least understood components of the Titan atmosphere. No published models to date directly address the thermal, radiative, and collisional accommodation properties of the haze in constraining the atmospheric thermal structure (24, 26, 32).

The UVIS occultation experiment at the Titan T_B flyby thus shows the presence of a mesopause with a relatively deep minimum in temperature in the dark south latitude atmosphere. The inference is that this is a structure similar to Earth's mesopause, where the effect of radiative cooling in reducing atmospheric temperature is balanced by the downward flow of heat from the thermosphere. Normalizing to the density of N₂ established at 1174 km by the INMS experiment, our predicted density of N₂ at 615 km using the UVIS temperature profile is 4 × 10¹³ cm⁻³. This is a high value, and it remains to be seen whether this is compatible with the density profile from the surface up to 200 km determined by the Voyager radio occultation or whether atmospheric dynamics seriously affects vertical distribution in local time (30, 31). Sicardy *et al.* (31) report the presence of a strong 200 m s⁻¹ jet at northern latitudes, tapering to zero in south latitudes, and a well-confined inversion layer with a temperature increase of more than 15 K in a span of 6 km near 510 km, in ground-based stellar occultation observations spanning the altitude range 250 to 550 km. A layer of the reported subscale height size (31) would be attenuated in the UVIS T_B experi-

Fig. 4. The density distribution of CH₄ derived from the reduction of the UVIS Shaula occultation data is compared with the INMS (21) inbound values and the ingress-egress extraction by Vervack *et al.* (4, 29) from the Voyager occultation. The CH₄ densities in the Wilson and Atreya (24) model are also plotted at selected altitudes. (See Table 1.)

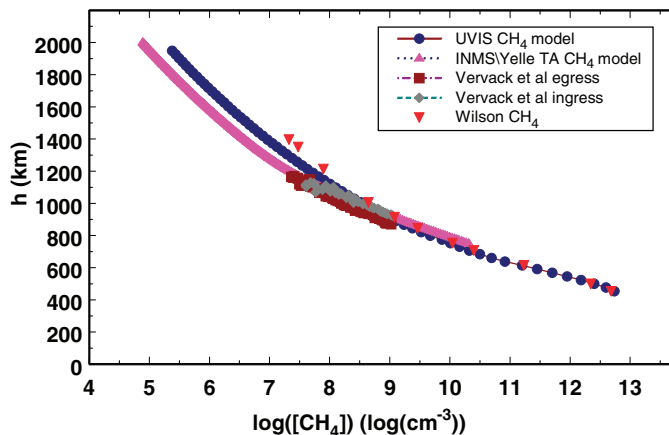


Table 1. Derived species densities at selected altitudes from the Cassini UVIS experiment compared with model calculations by Wilson and Atreya (24).

Altitude (km)		Number density (cm ⁻³)					
<i>h</i>		CH ₄ *	C ₂ H ₂ †	C ₂ H ₄ †	C ₂ H ₆ †	C ₄ H ₂ †	HCN†
454	‡	5.5 × 10 ¹²					
	§	5.5 × 10 ¹²	3.6 × 10 ⁹	1.3 × 10 ⁸	6.0 × 10 ⁹	4.9 × 10 ⁶	7.4 × 10 ⁸
500	‡	2.5 × 10 ¹²					
	§	2.2 × 10 ¹²	1.8 × 10 ⁹	1.4 × 10 ⁸	2.7 × 10 ⁹	6.9 × 10 ⁶	4.1 × 10 ⁸
615	‡	1.6 × 10 ¹¹	1.4 × 10 ⁹				3.1 × 10 ⁸
	§	1.7 × 10 ¹¹	3.2 × 10 ⁸	1.2 × 10 ⁸	3.6 × 10 ⁸	6.5 × 10 ⁶	1.0 × 10 ⁸
707	‡	2.1 × 10 ¹⁰	3.9 × 10 ⁸		2.8 × 10 ⁸		3.3 × 10 ⁸
	§	2.6 × 10 ¹⁰	9.9 × 10 ⁷	8.5 × 10 ⁷	1.1 × 10 ⁸	2.4 × 10 ⁶	4.3 × 10 ⁷
753	‡	1.0 × 10 ¹⁰	¶	¶	2.2 × 10 ⁸	1.4 × 10 ⁷	2.1 × 10 ⁸
	§	1.1 × 10 ¹⁰	5.9 × 10 ⁷	7.1 × 10 ⁷	6.7 × 10 ⁷	1.4 × 10 ⁶	3.0 × 10 ⁷
845	‡	2.4 × 10 ⁹	1.7 × 10 ⁸	6.9 × 10 ⁷	6.8 × 10 ⁷	9.7 × 10 ⁶	5.3 × 10 ⁷
	§	2.7 × 10 ⁹	2.3 × 10 ⁷	4.1 × 10 ⁷	2.3 × 10 ⁷	4.0 × 10 ⁵	1.7 × 10 ⁷
914	‡	9.6 × 10 ⁸	5.1 × 10 ⁷	4.6 × 10 ⁷	4.1 × 10 ⁷	9.4 × 10 ⁶	4.1 × 10 ⁷
	§	1.2 × 10 ⁹	1.2 × 10 ⁷	2.3 × 10 ⁷	9.0 × 10 ⁶	1.4 × 10 ⁵	1.1 × 10 ⁷
1006	‡	3.3 × 10 ⁸	2.0 × 10 ⁷	2.5 × 10 ⁷	2.6 × 10 ⁷	4.3 × 10 ⁶	3.2 × 10 ⁷
	§	4.5 × 10 ⁸	4.5 × 10 ⁶	8.8 × 10 ⁶	2.4 × 10 ⁶	3.5 × 10 ⁴	5.4 × 10 ⁶
1213	‡	4.3 × 10 ⁷		¶			
	§	8.0 × 10 ⁷	4.9 × 10 ⁵	8.0 × 10 ⁵	1.4 × 10 ⁵	9.5 × 10 ²	6.2 × 10 ⁵
1350	‡	8.3 × 10 ⁷		9.3 × 10 ⁶			
	§	3.0 × 10 ⁷	1.2 × 10 ⁵	1.7 × 10 ⁵	2.6 × 10 ⁴	7.3 × 10 ²	1.4 × 10 ⁵
1397	‡	1.3 × 10 ⁷		¶			
	§	2.2 × 10 ⁷	7.2 × 10 ⁴	1.0 × 10 ⁵	1.5 × 10 ⁴	3.1 × 10 ²	8.3 × 10 ⁴

*UVIS values estimated uncertainty < ±20%. †UVIS values column systematic uncertainties as large as 100%. Point-to-point uncertainties ~30%. ‡UVIS data values. §Wilson and Atreya model (24). ||Densities too low to measure. ¶Densities not calculated.

ment. It is clear that the atmosphere in the range up to 600 km is a very complex system that will have to be examined over latitude and season to be understood.

References and Notes

1. L. W. Esposito *et al.*, *Science* **307**, 1251 (2005).
2. Materials and methods are available as supporting material on Science Online.
3. G. R. Smith *et al.*, *J. Geophys. Res.* **87**, 1351 (1982).
4. R. J. Vervack Jr., B. R. Sandel, D. F. Strobel, *Icarus* **170**, 91 (2004).
5. F. M. Flasar, *Planet. Space Sci.* **46**, 1109 (1998).
6. F. M. Flasar, *Planet. Space Sci.* **46**, 1125 (1998).
7. C. C. Porco *et al.*, *Nature* **434**, 159 (2005).
8. G. H. Mount, H. W. Moos, *Astrophys. J.* **224**, L35 (1978).
9. G. H. Mount, E. S. Warden, H. W. Moos, *Astrophys. J.* **214**, L47 (1977).
10. H. Sun, G. L. Weisler, *J. Chem. Phys.* **23**, 1160 (1955).
11. H. Okabe, *J. Chem. Phys.* **75**, 2772 (1981).
12. C. Y. R. Wu, F. Z. Chen, D. L. Judge, *J. Geophys. Res.* **106**, 7629 (2001).
13. F. Z. Chen, C. Y. R. Wu, *J. Quant. Spectrosc. Radiat. Transf.* **85**, 195 (2004).
14. C. Y. R. Wu, F. Z. Chen, D. L. Judge, *J. Geophys. Res. Planets* **109** (E7), E07S15; doi:10.1029/2003JE002180 (2004).
15. G. Cooper, G. R. Burton, C. E. Brion, *J. Electron Spectrosc. Relat. Phenom.* **73**, 139 (1995).
16. J. W. Au, G. Cooper, G. R. Burton, T. N. Olney, C. E. Brion, *Chem. Phys.* **173**, 209 (1993).
17. J. A. Nuth, S. Glicker, *J. Quant. Spectrosc. Radiat. Transfer* **28**, 223 (1982).
18. T. Nagata, T. Kondow, Y. Ozaki, K. Kuchitsu, *Chem. Phys.* **57**, 45 (1981).
19. J. A. R. Samson, G. N. Haddad, *J. Opt. Soc. Am.* **64**, 47 (1974).
20. J. A. R. Samson, G. N. Haddad, T. Masuoka, P. N. Pareek, *J. Chem. Phys.* **90**, 6925 (1989).
21. R. V. Yelle, personal communication.
22. D. F. Strobel, M. E. Summers, X. Zhu, *Icarus* **100**, 512 (1992).
23. J. H. Waite Jr. *et al.*, *Science* **308**, 982 (2005).
24. E. H. Wilson, S. K. Atreya, *J. Geophys. Res.* **109**, E06002; doi:10.1029/2003JE002181 (2004).
25. Y. L. Yung, M. Allen, J. P. Pinto, *Astrophys. J. (suppl.)* **55**, 465 (1984).
26. A. J. Friedson, Y. L. Yung, *J. Geophys. Res.* **89**, 85 (1984).
27. G. F. Lindal *et al.*, *Icarus* **53**, 348 (1983).
28. R. V. Yelle, D. F. Strobel, E. Lellouch, D. Gautier, *Eur. Space Agency Spec. Publ.*, *ESASP 1177*, 243 (1997).
29. D. F. Strobel, personal communication.
30. I. C. F. Muller, R. V. Yelle, *Geophys. Res. Lett.* **29**, 2139 (2002).
31. B. Sicardy *et al.*, *AAS/DPS 36.22065* (2004).
32. E. Lellouch, D. M. Hunten, G. Kockarts, A. Coustenis, *Icarus* **83**, 308 (1990).
33. The authors thank H. Waite and R. Yelle of the INMS team, D. Strobel for useful comments and for providing data and calculations, E. Wilson for useful discussion and model densities, and L. Bloom for work on the manuscript. This work is one part of the Cassini UVIS investigation supported by the NASA/Jet Propulsion Laboratory Cassini mission.

Supporting Online Material

www.sciencemag.org/cgi/content/full/308/5724/978/DC1

Materials and Methods
Figs. S1 and S2

3 March 2005; accepted 14 April 2005
10.1126/science.1111790

REPORT

Ion Neutral Mass Spectrometer Results from the First Flyby of Titan

J. Hunter Waite Jr.,¹ Hasso Niemann,² Roger V. Yelle,³ Wayne T. Kasprzak,² Thomas E. Cravens,⁴ Janet G. Luhmann,⁵ Ralph L. McNutt,⁶ Wing-Huen Ip,⁷ David Gell,¹ Virginie De La Haye,¹ Ingo Müller-Wordag,⁸ Brian Magee,¹ Nathan Borggren,³ Steve Ledvina,⁵ Greg Fletcher,¹ Erin Walter,¹ Ryan Miller,¹ Stefan Scherer,¹ Rob Thorpe,⁹ Jing Xu,¹ Bruce Block,¹ Ken Arnett¹

The Cassini Ion Neutral Mass Spectrometer (INMS) has obtained the first in situ composition measurements of the neutral densities of molecular nitrogen, methane, molecular hydrogen, argon, and a host of stable carbon-nitrile compounds in Titan's upper atmosphere. INMS in situ mass spectrometry has also provided evidence for atmospheric waves in the upper atmosphere and the first direct measurements of isotopes of nitrogen, carbon, and argon, which reveal interesting clues about the evolution of the atmosphere. The bulk composition and thermal structure of the moon's upper atmosphere do not appear to have changed considerably since the Voyager 1 flyby.

This Report documents neutral composition measurements made with the INMS during the first low-altitude pass through Titan's upper atmosphere by the Cassini-Huygens spacecraft on 26 October 2004. During the ± 15 min before and after its closest approach, INMS acquired a rich data set of information on

Titan's atmospheric composition and structure covering an altitude range from 3000 to 1174 km. The closest approach occurred at 38.774° latitude, 88.45° west longitude at a solar local time of 16.753 hours. The highest priority objective of the Cassini orbiter during the first flyby was to measure the densities of the major atmospheric constituents N₂ and CH₄ and the inferred thermal structure between 1174 and 2000 km, because these data were important in planning the Huygens probe insertion and subsequent Cassini orbiter flybys. However, these measurements and subsequent analysis yielded substantial scientific results, including (i) the existence of large-amplitude (~ 10 K) and large-spatial scale (~ 180 km) atmospheric waves between 1100 and 1500 km, (ii) the identification of a suite of carbon-nitrile compounds at higher altitudes than anticipated (~ 1200 km), and (iii) the determination of the isotopic ratios of nitrogen in N₂, carbon in

CH₄, and the abundance of ⁴⁰Ar as well as an upper limit for the mixing ratio of ³⁶Ar. We begin with a brief description of the instrument, then present the data set, and finish with a discussion of the major results enumerated above.

INMS is a dual-ion source quadrupole mass spectrometer covering the mass range of 0.5 to 8.5 and 11.5 to 99.5 daltons (1, 2). The dual-source design combines classic closed and open ionization source configurations designed to measure inert species and reactive species and ions, respectively. The primary data reported in this paper were obtained with the closed source, which is designed to measure nonreactive atmospheric gases. In the closed source, the neutral gas flows into a spherical antechamber where it thermally accommodates with the walls of the antechamber before flowing through a transfer tube to an electron ionization source; there, the gas is ionized by an electron impact at 70 eV. The high flyby velocity of the Cassini spacecraft with respect to Titan (~ 6 km s⁻¹) produces a dynamic pressure enhancement in the antechamber, which increases sensitivity (1, 2). Reactive species are not measured in this configuration.

Ionization of the primary constituents N₂ and CH₄ by the electron ionization source produced not only the primary ions N₂⁺ and CH₄⁺ but also dissociative fragments (over-

¹Department of Atmospheric, Oceanic, and Space Sciences, University of Michigan, Ann Arbor, MI 48109-2143, USA. ²NASA Goddard Space Flight Center, Greenbelt, MD 20771, USA. ³Lunar and Planetary Laboratory, University of Arizona, 1629 East University Boulevard, Tucson, AZ 85721-0092, USA. ⁴Department of Physics and Astronomy, University of Kansas, Lawrence, KS 66045, USA. ⁵Space Sciences Laboratory, University of California, Berkeley, CA 94720, USA. ⁶Applied Physics Laboratory, Johns Hopkins University, Laurel, MD 20723, USA. ⁷Institute of Astronomy, National Central University, Chung-Li 32054, Taiwan. ⁸Space and Atmospheric Physics Group, Imperial College, London SW7 2BW, UK. ⁹Southwest Research Institute, Post Office Drawer 28510, San Antonio, TX 78228-0510, USA.